METEOROLOGICAL
- 2 OCT 1978
LIBRARY

137847

MET O 11 TECHNICAL NOTE NUMBER 114

# Investigations of a two-level linear baroclinic instability model

by

S. J. Foreman

Met O 11
Meteorological Office
London Road
Bracknell
Berkshire

September 1978

NOTE: This paper has not been published. Permission to quote from it should be obtained from the Assistant Director of the above Meteorological Office branch.

FH33

## 1. Introduction

Baroclinic instability is a mechanism for the growth of mid-latitude depressions and their associated frontal systems. It is thus important that this phenomenon is understood, so that it may be correctly modelled by forecasting techniques. Many studies of this topic have been performed, some of the better known being those of Eady (1949), Charney (1947), and Green (1960).

Since the equations of motion for the atmosphere are capable of describing many types of wave, studies of baroclinic instability must contain simplifications in their formulations in order to extract the waves of interest. The approach used to derive analytic solutions is usually to consider the quasi-geostrophic equations and solve them under conditions which make the mathematics tractable. Green (1960) and Brown (1969) were less stringent in their imposed conditions and used numerical techniques to integrate the quasi-geostrophic equations. Simmons and Hoskins (1976) performed integrations with a full hemispheric model to investigate the baroclinic instability problem.

This study uses a technique intermediate to the last two mentioned. The linearised forms of the primitive equations are used, but motion is constrained to be independent of the meridional coordinate.

## 2. The Primitive Equations

### 2.1 Sigma coordinates

Use of

$$\sigma = \frac{\text{Pressure}}{\text{Surface Pressure}} = \frac{p}{p_*} \tag{2.1.1}$$

as vertical coordinate leads to the following form for the equations of motion. (See Haltiner (1971) for further details).

$$\frac{Du}{Dt} + fv + \frac{\partial \Phi}{\partial x} + RT \frac{\partial}{\partial x}(\ln(p_*)) = 0 \tag{2.1.2}$$

$$\frac{Dv}{Dt} - fu + \frac{\partial \Phi}{\partial y} + RT \frac{\partial}{\partial y}(\ln(p_*)) = 0 \tag{2.1.3}$$

$$\frac{DT}{Dt} - \frac{RT\omega}{p_* \sigma} = 0 \tag{2.1.4}$$

$$\frac{Dp_*}{Dt} + p_* \left( \frac{\partial u}{\partial x} + \frac{\partial v}{\partial y} + \frac{\partial \dot{\sigma}}{\partial \sigma} \right) = 0 \tag{2.1.5}$$

$$\frac{\partial \Phi}{\partial \sigma} + \frac{RT}{\sigma} = 0 \tag{2.1.6}$$

where $\frac{D}{Dt} = \frac{\partial}{\partial t} + u\frac{\partial}{\partial x} + v\frac{\partial}{\partial y} + \dot{\sigma}\frac{\partial}{\partial \sigma}$,

$\dot{\sigma} = \frac{D\sigma}{Dt}$, $\omega = \frac{Dp}{Dt}$,

$R = R/c_p$,

and $(\ )_*$ denotes a surface value.

Equation (2.1.6) has been derived from the vertical equation of motion by using the hydrostatic assumption.

Using the boundary conditions

$$\dot{\sigma} = 0 \quad \text{at} \quad \sigma = 0, 1$$

it is possible to show that

$$p_* \dot{\sigma} = \sigma \int_0^1 \nabla \cdot (p_* \underset{\sim}{v})\, d\sigma - \int_0^\sigma \nabla \cdot (p_* \underset{\sim}{v})\, d\sigma \tag{2.1.7}$$

and

$$\omega = \sigma \underset{\sim}{v} \cdot \nabla p_* - \int_0^\sigma \nabla \cdot (p_* \underset{\sim}{v})\, d\sigma \tag{2.1.8}$$

## 2.2 Vorticity and divergence forms of the equations.

Differentiating (2.1.2) and (2.1.3) with respect to $x$ and with respect to $y$ and combining the results leads to their vorticity and divergence forms.

$$\frac{D\zeta}{Dt} + (\zeta + f_0)\mathcal{D} + \left(\frac{\partial \dot{\sigma}}{\partial x}\frac{\partial v}{\partial \sigma} - \frac{\partial \dot{\sigma}}{\partial y}\frac{\partial u}{\partial \sigma}\right) + \beta v + R\left[\frac{\partial T}{\partial x}\frac{\partial \ln(f_x)}{\partial y} - \frac{\partial T}{\partial y}\frac{\partial \ln(f_x)}{\partial x}\right] = 0 \qquad (2.2.1)$$

$$\frac{D\mathcal{D}}{Dt} + \mathcal{D}^2 + 2\left(\frac{\partial v}{\partial x}\frac{\partial u}{\partial y} - \frac{\partial u}{\partial x}\frac{\partial v}{\partial y}\right) + \left(\frac{\partial \dot{\sigma}}{\partial x}\frac{\partial u}{\partial \sigma} + \frac{\partial \dot{\sigma}}{\partial y}\frac{\partial v}{\partial \sigma}\right) - f_0\zeta + \beta u + \nabla^2\phi + RT\nabla^2\ln(f_x) + R\left[\frac{\partial T}{\partial x}\frac{\partial \ln(f_x)}{\partial x} + \frac{\partial T}{\partial y}\frac{\partial \ln(f_x)}{\partial y}\right] = 0 \qquad (2.2.2)$$

where $$\mathcal{D} = \frac{\partial u}{\partial x} + \frac{\partial v}{\partial y}$$

$$\zeta = \frac{\partial v}{\partial x} - \frac{\partial u}{\partial y}$$

and the $\beta$-plane approximation has been incorporated by taking the coriolis parameter as

$$f = f_0 + \beta y, \quad \beta y \ll f_0 \qquad (2.2.3)$$

## 2.3 Boundary conditions.

The upper and lower boundary conditions for the vertical motion are

$$\dot{\sigma} = 0 \quad \text{at} \quad \sigma = 0, 1 \qquad (2.3.1)$$

On the assumption that the lower boundary is formed by a horizontal surface, the additional condition

$$\phi_x = 0 \qquad (2.3.2)$$

may be imposed.

## 3. The Model

### 3.1 General Description.

The model to be employed is a simplified form of the primitive equations of Section 2. It is assumed that the area under consideration is of infinite extent, and that the only variations in the meridional direction are those implicit in the basic state of Section 3.2. Equations (2.2.1), (2.2.2) and (2.1.4)-(2.1.6) are linearised in Section 3.3, and it is assumed that the motions are such as to maintain the conditions assumed in the linearised equations. Finally it is assumed that the perturbations to the basic state of Section 3.2 are sinusoidal.

### 3.2 The basic state.

It is assumed that the basic state of the model is one of a zonal flow, $U$, and associated temperature, $T_m$, which do not vary in the zonal direction. In order that the basic state be in geostrophic balance, there must be a horizontal temperature gradient, $\frac{\partial T_m}{\partial y}$. It is assumed that the meridional and vertical compoents of velocity in the basic state are identically zero.

The further assumption of uniform surface pressure, $p_0$, leads to the equations

$$f_0 U + \frac{\partial \Phi}{\partial y} = 0 \qquad (3.2.1)$$

$$\frac{\partial \Phi}{\partial \sigma} + \frac{R T_m}{\sigma} = 0 \qquad (3.2.2)$$

for the basic state.

Elimination of $\Phi$, the geopotential of the basic state, gives

$$f_0 \frac{\partial U}{\partial \ln(\sigma)} - R \frac{\partial T_m}{\partial y} = 0 \qquad (3.2.3)$$

Since $p_0$ = constant, it must be the case that

$$U_* = 0 \qquad (3.2.4)$$

It is useful to consider two special instances of the basic state. In the case

$$\frac{\partial T_m}{\partial y} = \text{constant}$$

integration of (3.2.3) gives

$$U(\sigma) = \frac{R}{f_o} \frac{\partial T_m}{\partial y} \ln(\sigma) \qquad (3.2.5)$$

which, on the assumption of a height-pressure relationship of the form

$$z = -h \ln\left(p/p_*\right)$$

gives

$$U(z) = -\frac{R}{f_o} \frac{\partial T_m}{\partial y} \frac{z}{h} \qquad (3.2.6)$$

ie $U$ is linear in $z$. This profile is that widely used in the literature. (Charney, 1949; Geisler and Garcia, 1977).

The next special case to consider is a profile of $U$ which is linear in $\sigma$,

$$\text{i.e.} \qquad U = S(1-\sigma) \qquad (3.2.7)$$

This gives

$$U = S\left(1 - \exp\left\{-\frac{z}{h}\right\}\right) \qquad (3.2.8)$$

The profiles (3.2.6) and (3.2.8) are shown in Fig 1.

3.3 The linearised equations

The system of equations (2.2.1), (2.2.2), (2.1.4)-(2.1.6) may be linearised on the assumption that the motion consists of a basic

state with small perturbations imposed upon it. It is assumed that the perturbation quantities are independent of the meridional coordinate. Using the basic state of 3.2, the system takes the following form.

$$\frac{\partial \zeta}{\partial t} + U\frac{\partial \zeta}{\partial x} + \beta v + f_0 D - \frac{R}{p_0}\frac{\partial T_m}{\partial y}\frac{\partial p_s}{\partial x} = 0 \qquad (3.3.1)$$

$$\frac{\partial D}{\partial t} + U\frac{\partial D}{\partial x} + \frac{\partial \dot{\sigma}}{\partial x}\frac{\partial U}{\partial \sigma} - f_0\zeta + \beta u + \frac{\partial^2 \phi}{\partial x^2} + \frac{RT}{p_0}\frac{\partial^2 p_s}{\partial x^2} = 0 \qquad (3.3.2)$$

$$\frac{\partial \phi}{\partial \ln \sigma} + RT = 0 \qquad (3.3.3)$$

$$\frac{\partial p_s}{\partial t} + U\frac{\partial p_s}{\partial x} + p_0\left(\frac{\partial u}{\partial x} + \frac{\partial \dot{\sigma}}{\partial \sigma}\right) = 0 \qquad (3.3.4)$$

$$\frac{\partial T}{\partial t} + U\frac{\partial T}{\partial x} + v\frac{\partial T_m}{\partial y} + \dot{\sigma}\frac{\partial T_m}{\partial \sigma} - \frac{RT_m\omega}{p_0\sigma} = 0 \qquad (3.3.5)$$

where $p_0$, $U$, $T_m$ represent the basic state; $\zeta = \frac{\partial v}{\partial x}$, $D = \frac{\partial u}{\partial x}$, $u$, $v$, $\dot{\sigma}$, $T$, $p_s$, $\omega$ are the perturbations to it.

The linearised conditions on $\dot{\sigma}$ and $\omega$ are

$$p_0\dot{\sigma} = \sigma\int_0^1\left[U\frac{\partial p_s}{\partial x} + p_0\frac{\partial u}{\partial x}\right]d\sigma - \int_0^\sigma\left[U\frac{\partial p_s}{\partial x} + p_0\frac{\partial u}{\partial x}\right]d\sigma \qquad (3.3.6)$$

$$\omega = \sigma U\frac{\partial p_s}{\partial x} - \int_0^\sigma\left[U\frac{\partial p_s}{\partial x} + p_0\frac{\partial u}{\partial x}\right]d\sigma \qquad (3.3.7)$$

(3.3.4) can be integrated over the atmosphere to give

$$\frac{\partial p_s}{\partial t} + \frac{\partial p_s}{\partial x}\int_0^1 U\,d\sigma + p_0\int_0^1 u\,d\sigma = 0 \qquad (3.3.8)$$

where the boundary conditions

$$\dot{\sigma} = 0 \quad \text{at} \quad \sigma = 0, 1 \qquad (3.3.9)$$

are used to eliminate $\int_0^1 \frac{\partial \dot{\sigma}}{\partial \sigma} d\sigma$ .

3.4 Solution of the equations.

Solutions to (3.3.1)-(3.3.8) are sought which have a sinusoidal wave structure in the zonal direction. These are of the form

$$u = u\, e^{i(kx + \alpha t)} \qquad \text{etc,}$$

where $k$ is the wave number of the wave ( $2\pi$ /wavelength) and $\alpha/k$ its phase speed. $u$ and $\alpha$ may be complex, but $k$ is confined to real (positive) values.

The equations are solved by using a two-level model with finite differencing in the vertical. The finite difference scheme adopted is a modified form of that of Corby, Gilchrist and Newson (1972).

The finite difference forms of (3.3.1)-(3.3.1)-(3.3.8) are thus

$$\frac{\alpha}{k}(iv) = (-U + \beta/k^2)(iv) - f_0/k\,(u) + \frac{R}{f_0 k}\frac{\partial T_m}{\partial y}(p_x) \tag{3.4.1}$$

$$\frac{\alpha}{k}(u) = (-U + \beta/k^2)(u) - \frac{f_0}{k}(iv) + i\,\overline{\frac{\dot{\sigma}\delta_\sigma U}{k}}^{\sigma} - \phi - \frac{RT_m}{p_0}(p_x) \tag{3.4.2}$$

$$\frac{\alpha}{k}(T) = -U(T) + \frac{1}{k}\frac{\partial T_m}{\partial y}(iv) + i\,\overline{\frac{\dot{\sigma}\delta_\sigma T_m}{k}}^{\sigma} + i\frac{RT_m\omega}{kp_0\sigma} \tag{3.4.3}$$

$$\frac{\alpha}{k}(p_x) = -\sum_{s=1}^{2}(p_0 u_s + p_x U_s)\Delta\sigma \tag{3.4.4}$$

where $$\phi_n = \phi_s + \sum_{s=n}^{1}\left[\tfrac{1}{2}R(T_s + T_{s+1})\ln\left(\frac{\sigma_{s+1}}{\sigma_s}\right)\right] - RT_2 \ln\sigma_2 \tag{3.4.5}$$

$$p_0\dot{\sigma}_{n+1/2} = ikU_{n+1/2}\sum_{s=1}^{2}(p_0 u_s + p_x U_s)\Delta\sigma - ik\sum_{s=1}^{n}(p_0 u_s + p_x U_s)\Delta\sigma \tag{3.4.6}$$

$$-\left(\frac{RT_m\omega}{p_0\sigma}\right)_n = -ikRT_{m,n}\left\{\tfrac{1}{2}\ln\left(\frac{\sigma_{n+1}}{\sigma_n}\right)\sum_{s=1}^{n}\left(u_s + \frac{p_x}{p_0}U_s\right) + \tfrac{1}{2}\ln\left(\frac{\sigma_n}{\sigma_{n-1}}\right)\sum_{s=1}^{n-1}\left(u_s + \frac{p_x}{p_0}U_s\right) - U_n\frac{p_x}{p_0}\right\} \tag{3.4.7}$$

and where $$\overline{a}^{\sigma} = \tfrac{1}{2}\left(a_{n+1/2} + a_{n-\frac{1}{2}}\right)$$

$$\delta_\sigma a = \frac{a_{n+1/2} - a_{n-1/2}}{\Delta\sigma}$$

The boundary conditions $\dot{\sigma} = 0$ at $\sigma = 0, 1$ are used in the derivation of (3.4.6) and (3.4.7).

When finding the vertical velocity at level 2, $\omega_2$, it is necessary to consider the influence of the lower boundary. This is done by writing

$$-\left(\frac{RT_m\omega}{p\sigma}\right)_2 = -ikRT_{m2}\left\{\tfrac{1}{2}\ln\left(\tfrac{1}{\sigma_2}\right)\sum_{s=1}^{2}\left(u_s + \frac{p_x}{p_0}U_s\right) + \tfrac{1}{2}\ln\left(\frac{\sigma_2}{\sigma_1}\right)\sum_{s=1}^{1}\left(u_s + \frac{p_x}{p_0}U_s\right) - U_2\frac{p_x}{p_0}\right\} - \tfrac{1}{2}ikRT_{m*}\ln\left(\tfrac{1}{\sigma_2}\right)\sum_{s=1}^{2}\left(u_s + \frac{p_x}{p_0}U_s\right) \qquad (3.4.8)$$

The distribution of the variables and levels is shown in Figure 2.

The system (3.4.1) to (3.4.4), after substitution from (3.4.5) to (3.4.8), may, given $k$, be solved as an eigenvalue problem for $c/k$ involving seven equations. This can be done using standard computer packages. The eigenvectors giving the values of $u$, $v$, $T$ and $p_x$ corresponding to each eigenvalue can also be found to give the vertical structure of the perturbations.

Of the seven eigenvalues found, four will correspond to gravity waves and the other three will be of interest in the present study.

## 4. Results

### 4.1 Constant Temperature Gradient

This section will be concerned with describing the baroclinic waves produced within the model when a uniform horizontal temperature gradient is applied. Most attention will be given to those waves which are less than 10,000 km long, although some outside this range will be mentioned.

Figure 3 shows the variation in the growth rates of unstable waves with varying wave number under conditions of different static stability. In both cases illustrated the horizontal temperature gradient has a uniform value of $-10^{-5}$ K $m^{-1}$. It can be seen that there are two wavenumbers at which the growth-rate attains a local maximum within the range of wavenumbers shown. For convenience, the peak occurring at the larger wavenumber (shorter wavelength) will be referred to as the "TM" mode, the other being the "BM" mode. It is apparent that increasing the static stability of the atmosphere reduces the growth-rates of the baroclinic waves. Closer inspection reveals that the effects of static stability on the TM mode are greater than on the BM mode.

In addition to varying the static stability of the atmosphere it is possible to vary the horizontal temperature gradient. The results of doing this are shown in figure 4. It can be seen that as the wind shear, (and hence the horizontal temperature gradient), decreases, the TM and BM modes both become less unstable. In the case shown the BM mode is stable to greater wind-shears than is the TM mode, although by choosing a different static stability for the basic state it is possible to reverse this. Considering the TM mode, increasing the wind difference for a given wavenumber from zero leads to the following sequence. Initially the flow is stable, but as the shear increases beyond a certain value the baroclinic waves become unstable. The growth-rate increases with the wind

shear until it attains a maximum value. Further increasing the wind shear reduces the growth-rate until the waves again become stable and remain so as the shear increases further. This is only discernable at large values of the wavenumber in figure 4, but it is present for all wavenumbers in the TM mode for sufficiently large wind shears.

Calculation of the eigenvectors of the system in section 3.4 for the eigenvalues corresponding to baroclinic waves enables the structure of the waves to be investigated. Figures 5 and 6 show the structure of the eigenvectors for selected waves. The major distinction between the TM and BM modes lies in the temperature perturbation, and is thus reflected in the geopotential variation. In the TM mode the upper level perturbation is displaced to the west from that at the lower level, and its amplitude is less. In the BM mode there is only a small phase difference between the two levels, the upper level perturbation being slightly to the east of that at the lower level. The meridional velocity perturbation slopes westward with height for all unstable wavelengths. Associated with the meridional velocity is the "pseudo-geopotential", ( $\phi'$ ), which is that form of the geopotential driving the geostrophic wind, defined by

$$\phi' = \phi + \frac{RT_m}{p_0} p_x$$

This also slopes westward with height for all unstable wavelengths. The geostrophic value of the meridional wind in the BM mode differes by 10% of its actual value, but in the TM mode the difference is up to 36% at the lower level. In both cases the model wind is stronger than the geostrophic wind. In the TM mode, the upper wind is within 10% of being geostrophic. The zonal velocity perturbation in both cases is such that the upper and lower levels are out of phase by approximately $180^{\circ}$. These velocities, together with the surface pressure perturbation, may be used to determine the vertical velocity from (3.4.6). The values of this for selected wavelengths are shown in Table 1.

| Wavelength (km) | Vertical velocity ( =0.25) | | Vertical velocity ( =0.75) | |
|---|---|---|---|---|
| | mb $s^{-1}$ | m $s^{-1}$ | mb $s^{-1}$ | m $s^{-1}$ |
| 2500 | $1.125 \times 10^{-7}$ | $2.9 \times 10^{-6}$ | $3.280 \times 10^{-7}$ | $3.5 \times 10^{-6}$ |
| 3250 | $5.280 \times 10^{-8}$ | $1.4 \times 10^{-6}$ | $1.638 \times 10^{-7}$ | $1.7 \times 10^{-6}$ |
| 4750 | $5.686 \times 10^{-9}$ | $1.4 \times 10^{-7}$ | $2.084 \times 10^{-8}$ | $2.3 \times 10^{-7}$ |
| 5750 | $2.849 \times 10^{-9}$ | $7.1 \times 10^{-8}$ | $1.114 \times 10^{-8}$ | $1.2 \times 10^{-7}$ |
| 9000 | $1.308 \times 10^{-9}$ | $3.4 \times 10^{-8}$ | $3.780 \times 10^{-9}$ | $4.0 \times 10^{-8}$ |

Vertical velocities $\left(\frac{Dp}{Dt}\right)$ for a unit pressure perturbation amplitude (1 mb) for $T_{m1} = 220K$, $T_{m2} = 260K$, $T_{m*} = 280$ K; $\frac{\partial T_m}{\partial y} = -10^{-5} Km^{-1}$, $p_o = 1000$ mb. The values in m $s^{-1}$ are derived from the ICAO atmosphere and are given as a guide only.

TABLE 1

It can be seen that the vertical velocities in the TM mode are larger than those of the BM mode by a factor of ten.

Figure 7 shows the phase speeds of baroclinic waves for a horizontal temperature gradient of $-10^{-5}$K $m^{-1}$. The mathematics of the model are such that an unstable mode must occur in both a decaying and a growing form, so that the onset of instability corresponds to the merging of two neutral waves. It is from this merging that the previous terminology of TM and BM modes was derived. The investigations of section 4.2 lead to the identification of the stable waves shown in figure 7. This figure also shows the third mode of instability present in the model. Since this mode occurs at wavelengths of, or longer than, the circumference of the circle of latitude under consideration, this mode is unlikely to have any physical significance.

In the third, TB, mode, as in the TM mode, the meridional velocity differs greatly from the geostrophic value, by as much as 50% of the model meridional wind. In this case, as in the TM mode, the temperature

and geopotential perturbations at the upper level are to the west of those at the lower level. The meridional velocity differs in phase between the two levels by approximately $180^{\circ}$, the lower level leading as in the other two modes.

4.2 Velocity of basic state linear in sigma

The previous section described the structure of unstable waves with the basic state of (3.2.5). Section 3.2 also described a second basic state (3.2.7), and it is with perturbations about this state that the present section is concerned. The TB mode waves of very long wavelength are similar to those of the previous section, and are not discussed here.

Figure 8 shows the variation of the growth-rate of unstable modes with wind shear and wavenumber. These results differ from those of section 4.1 in that only one mode of instability is present for a given wind shear. In addition, the growth-rate at short wavelengths does not decrease as the wind shear increases beyond a critical value, unlike the TM mode of the previous section. This is consistent with the BM mode discussed previously, and investigation of the phase-velocities (not illustrated) confirms that this unstable mode is, indeed, of the BM type.

The structure of this single mode is, however, not compatible with that of the BM mode in the previous section. At short wavelengths (less than 4250 km in the case illustrated in figure 8) the temperature and geopotential perturbations at the upper level are to the west of those at the lower level, as in the case of the TM mode in section 4.1. For longer waves the structure is the same as for the BM mode of the previous section. When the meridional velocities are compared with their geostrophic values, the results again compare with the TM or BM mode of the previous section, according to whether the wave is shorter or longer than 4250 km. When the amplitudes of the temperature

perturbations are considered they are found to be larger at the lower level by a factor of between six and ten depending upon wavelength. This factor increases as the waves become longer. This is not in accord with the BM mode of section 4.1, but since in the present situation the horizontal temperature gradient at the lower level is more than ten times that the the upper level this result is reasonable.

The vertical velocities associated with this mode are shown in Table 2.

| Wavelength (km) | Vertical velocity ( =0.25) | | Vertical velocity ( =0.75) | |
|---|---|---|---|---|
| | mb $s^{-1}$ | m $s^{-1}$ | mb $s^{-1}$ | m $s^{-1}$ |
| 2250 | $3.625 \times 10^{-6}$ | $9.4 \times 10^{-5}$ | $1.166 \times 10^{-5}$ | $1.2 \times 10^{-4}$ |
| 3250 | $9.759 \times 10^{-7}$ | $2.5 \times 10^{-5}$ | $3.309 \times 10^{-6}$ | $3.5 \times 10^{-5}$ |
| 4500 | $4.229 \times 10^{-7}$ | $1.1 \times 10^{-5}$ | $1.528 \times 10^{-6}$ | $1.6 \times 10^{-5}$ |
| 6250 | $1.910 \times 10^{-7}$ | $4.9 \times 10^{-6}$ | $7.466 \times 10^{-7}$ | $7.9 \times 10^{-6}$ |
| 7750 | $1.141 \times 10^{-7}$ | $2.9 \times 10^{-6}$ | $4.427 \times 10^{-7}$ | $4.7 \times 10^{-6}$ |
| 9000 | $7.972 \times 10^{-8}$ | $2.1 \times 10^{-6}$ | $1.938 \times 10^{-7}$ | $2.1 \times 10^{-6}$ |

As table 1, but $U_1 = 45$ m $s^{-1}$, $U_2 = 15$ m $s^{-1}$.

TABLE 2

4.3 Other profiles

The results of investigations in which the horizontal temperature gradient at the upper level was varied from the value appropriate to the situation of section 4.1 to a value appropriate to a linear velocity profile are shown in figure 9. It can be seen that the growth rate of the TM mode decreases rapidly as the temperature gradient at

the upper level is reduced. This is accompanied by a shift of the shortwave cut off to smaller wavenumbers. As the upper temperature gradient is reduced further the cut-off returns to larger wavenumbers and the TM mode loses its identity.

When the short-wave cut-off is near its smallest wavenumber, (at a horizontal temperature gradient of approximately $0.7 \times 10^{-5} K\ m^{-1}$ at the upper level), the temperature perturbation is such that the upper level is to the east of the lower and is of greater amplitude. When this cut-off is at larger wavenumbers the temperature perturbation in its vicinity is of the opposite structure, namely larger at the lower level and the upper wave to the west of the lower one.

It can be seen that the transition of the growth-rate curve between its forms of the previous two sections is smooth, and consists of the decay of the TM mode accompanied by the movement to shorter wavelengths of the BM mode. It is also possible to see why, in the case of the linear velocity profile of section 4.2, the temperature perturbations at the lower level are larger than those at the upper one, whereas the opposite is true of the BM mode of section 4.1. This is consistent with the smooth change in the relative amplitudes as the horizontal temperature gradient at the upper level decreases. Since the north-south velocity component will lead to a temperature perturbation proportional to the horizontal temperature gradient, this effect is consistent with the meridional motion being important in the growth of the BM mode.

Another experiment was performed in which the horizontal temperature gradient increased with height. This result, which is not illustrated here, indicated the dominance of the TM mode until long wavelengths (6000 km), where the BM mode became effective until 7500 km. This case corresponded to $\frac{\partial T_m}{\partial y}_1 = -10^{-5}\ K\ m^{-1}$, $\frac{\partial T_m}{\partial y}_2 = -0.5 \times 10^{-5}\ K\ m^{-1}$

Experiments were also performed in which the variation of the coriolis parameter was set to zero and also reversed. Both had the effect of maintaining the mode which was initiated at the shortest wavelength. The growth-rate of this mode decreased slightly, but did not return to zero within the range of wavelengths of physical significance. Imposition of the coriolis terms appropriate to $15^{o}$N in the constant temperature gradient form of the model led to the only mode of instability being the TM mode, which showed marked dependence upon the wind shear. The maximum growth-rate occurred at 4250 km corresponding to a velocity difference of 25 m $s^{-1}$ between the two levels.

## 5. Discussion

Previous studies, such as those by Brown (1969) and James (1977), have produced a growth-rate curve which appears similar to that of this model. Both were able to identify one of their peaks with the 'Charney' mode of instability described in Charney (1947). Brown explained this second peak, at longer wavelengths than his first, in terms of barotropic instability. Since the present model has no meridional variation in the basic state this is not an explanation for one of the observed modes of instability. James likened his extra mode to Kelvin Helmholtz instability, and in particular found that it was present under conditions of no rotation. In the present case, putting $\beta = 0$ leads to a stable situation.

It is instructive to consider the case of no rotation in the present model, as it will enable an identification of the T, M and B waves. (3.4.1) to (3.4.4) become

$$\frac{\alpha}{R}(i\upsilon) = -U(i\upsilon) \qquad (5.0.1)$$

$$\frac{\alpha}{R}(u) = -Uu + i\overline{\frac{\delta\delta_\sigma U}{R}}^{\sigma} - \phi - \frac{RT_m}{p_0}p_x \qquad (5.0.2)$$

$$\frac{\alpha}{R}(T) = -UT + i\overline{\frac{\delta\delta_\sigma T_m}{R}}^{\sigma} + i\frac{RT_m}{p_0\sigma R}\omega \qquad (5.0.3)$$

$$\frac{\alpha}{k}(p_x) = -p_x \sum_{s=1}^{2} U_s \Delta\sigma - p_0 \sum_{s=1}^{2} u_s \Delta\sigma \qquad (5.0.4)$$

where $\sigma$ and $\omega$ may be written in terms of $u_s$, $U_s$ and $p_x$.

This uncouples (5.0.1) from the remaining equations. The only non-trivial solutions of (5.0.1) are

$$\frac{\alpha}{k} = U_s, \quad v_{3-s} = 0, \quad v_s \text{ arbitrary}, \quad s = 1, 2.$$

These can be seen to correspond to the $T$ and $B$ waves, which are thus 'vorticity' waves whose most important feature is meridional motion.

However, (5.0.2) to (5.0.4) may also be solved as a system with $v_1 = v_2 = 0$. This leads to a solution travelling with phase speed $(\alpha/k)_0$ which may be expected to be approximately $\sum_{s=1}^{2} U_s \Delta\sigma$ in cases where the average divergence is small. In addition solutions representing gravity waves are present.

The relevant solutions are of two distinct types. Those corresponding to the two levels of the model are vorticity waves in which the major element is the meridional motion, and the other is a divergence wave which owes its existence to vertical motions.

Introducing the rotation of the Earth results in waves of more complex form. The introduction of the coriolis term will produce a divergence into the vorticity dominated wave and vice versa. These in turn affect temperature structure of the waves by introducing advective and adiabatic effects into the motions which were previously absent.

Mathematically, although not physically, the same system results from letting the wavelength of the disturbances tend to zero. The foregoing is thus also true of very short waves. Hence, increasing the wavelength from zero will introduce vorticity into the divergence wave. This may become increasingly important until the wave can no longer remain in balance and becomes unstable. The phase speed at which this occurs will depend upon the basic state. This phase speed is found in the numerical solutions to correspond closely to the analytically determined mean zonal wind in those cases where this is sufficiently removed from

the numerically approximated mean as to enable the combination of the M and T or B modes. In the case of the linear velocity profile the phase speed at the onset of instability is less than the mean zonal wind which is also the calculated average. This is due to the need for two modes to interact in order to produce instabilities, and so the M mode must alter its phase speed from the mean value of the zonal wind. That the model should detect the presence of this level is not infeasible since the temperature gradient term carries information about the wind shear at each level.

Increasing the horizontal temperature gradient will amplify the effect of any meridional motions informing a temperature perturbation, so that an overall decrease of meridional velocity is to be expected in this situation. This will, in the case of an unstable divergence wave, lead to the divergence again being able to balance the wave as the effects due to the coriolis term acting on the meridional velocity will be decreased. Hence the divergence wave will become stabilised as the magnitude of the horizontal temperature gradient exceeds a certain limit, which will depend upon the wavelength and coriolis parameter $f$. This limit is increased for a given wavelength if the rate of rotation, and hence $f$, is increased.

This mode occurs even in the case of a velocity profile which is linear in sigma, but is absorbed into the BM mode in the case of the 2 level model, which is unable to resolve it. Using a greater number of levels it is possible to detect this mode in the case of a linear velocity profile. (Radford, personal communication).

Conventional studies of baroclinic waves are concerned primarily with the vorticity waves which correspond to the BM mode of section 4.1. These are usually found to become unstable at wavelengths shorter than those in this study, but the results summarised in figure 9 suggest that this is due to the presence of the divergence mode dominating the vorticity mode, rather than an absence of the vorticity mode from the shorter (2000 to 3000 km) wavelengths. A description of the mechanism of instability of

these waves can be found in Wallace and Hobbs (1977).

Finally, the TB mode of the two level model is the result of the interaction of its two vorticity waves. This corresponds to the physical situation in which the dominant influences are the coriolis effect and the horizontal temperature gradient. The wavelengths at which this mode occurs are such that the necessary conditions are unlikely to be attained in the atmosphere.

## 6. Conclusion

It has been shown that the linearised 2-level sigma-coordinate primitive equations are capable of describing three modes of instability under baroclinic conditions in a statically stable atmosphere. Baroclinicity is necessary for any of the modes to occur, but the conditions under which an individual mode can exist depend upon the mode being considered.

A barcclinic atmosphere is thus unstable on a wide range of length scales, but the amplitudes of the growth-rates are such that under conditions normally found in the atmosphere the dominant waves are on the length scales of observed depressions.

References


Brown, J 1969 A Numerical Investigation of Hydrodynamic Instability and Energy Conversions in the Quasi-geostrophic Atmosphere.
J Atmos. Sci. 26, 352-375.

Charney, J G 1947 The Dynamics of Long Waves in a Baroclinic Westerly Current.
J Met. 4, 135-162.

Corby, G A, Gilchrist, A Newson, R L 1972 A General Circulation Model of the Atmosphere Suitable for Long Period Integrations.
Q J Roy. Met. Soc. 98, 809-832.

Eady, E T 1949 Long Waves and Cyclone Waves.
Tellus 1, 33-52.

Geisler, J E, Garcia, R R 1977 Baroclinic Instability at Long Wavelengths on a $\beta$ -plane.
J Atmos. Sci. 34, 311,321.

Green, J S A 1960 A Problem in Baroclinic Instability.
Q J Roy. Met. Soc. 86, 237-251.

Haltiner, G J 1971 Numerical Weather Prediction.
John Wiley and Sons, Inc.
New York.

James, I N 1977 Stability of Flow in a Slowly Rotating 2-layer system.
Met O 21. Tech Note 7712.

Simmons, A J Hoskins, B J 1976 Baroclinic Instability on the Sphere: Normal modes of the Primitive and Quasi-geostrophic Equations.
J.Atmos. Sci. 33, 1454-1477.

Wallace, J M Hobbs, P V 1977 Atmospheric Science. An Introductory Survey.
Academic Press.
New York.

Legends

Figure 1 The velocity profiles used in the study plotted against $\sigma$, (a) and the geometric height, (b). The profile linear in sigma (solid line) is $U = 6(1 - \sigma)$, and the constant temperature gradient profile (dashed line) corresponds to $\frac{R}{f_0}\frac{\partial T_m}{\partial y} = -5/5$.

Figure 2 The distribution of variables used in the model. Those held explicitly are used to calculate those which are derived implicitly. The latter are in parentheses.

Figure 3 Growth-rate against wavenumber for baroclinic waves. The results for two static stabilities are shown: $T_{m1} = 214\,K$, $T_{m2} = T_{m*} = 264\,K$ (dashed line) and $T_{m1} = 220\,K$, $T_{m2} = T_{m*} = 260\,K$ (solid line). Both correspond to $f_0 = 10^{-4}\,s^{-1}$, $\beta = 1.5 \times 10^{-11}\,m^{-1}s^{-1}$, $p_0 = 1000\,mb$, $\frac{\partial T_m}{\partial y} = -10^{-5}\,K\,m^{-1}$.

Figure 4 Growth-rate against wavenumber and wind-difference between the two model layers corresponding to horizontal temperature gradients constant with height. $f_0 = 10^{-4}\,s^{-1}$, $\beta = 1.5 \times 10^{-11}\,m^{-1}s^{-1}$, $p_0 = 1000\,mb$, $T_{m1} = 220K$, $T_{m2} = T_{m*} = 260\,K$.

Figure 5 The vertical structure of waves corresponding to $\frac{\partial T_m}{\partial y} = -10^{-5}\,K\,m^{-1}$ under the conditions of figure 4, but $T_* = 250\,K$. The quantities shown are temperature (_____), meridional velocity (_._), geopoential (----), pseudo-geopotential (.....).

Figure 6 The variation of amplitude with height for the temperature, meridional velocity, and pseudo-geopotential perturbations under the conditions of figure 5. The amplitudes are scaled so that the maximum value at each wavelength is 1.

Figure 7 The interrelation of phase-speed and growth-rate for baroclinic waves. The conditions are those of figure 5. Phase speeds corresponding to stable waves are denoted by a dashed line, and those associated with unstable waves by a solid line. The growth-rates of unstable waves are shown by a dotted line.

Figure 8 Growth-rate against wind difference and wavenumber for a linear velocity profile of the basic state.

$T_{m1} = 214\ K$, $T_{m2} = 264\ K$, $T_{mx} = 264\ K$;

$f_0 = 10^{-4}\ s^{-1}$, $\beta = 1.5 \times 10^{-11}\ m^{-1} s^{-1}$

Figure 9 Growth-rate variation as the horizontal temperature gradient at the upper level varies, that at the lower level remaining fixed. $\left(\frac{\partial T_m}{\partial y}\right)_2 = -10^{-5}\ K\ m^{-1}$; $f_0 = 10^{-4}\ s^{-1}$, $\beta = 1.5 \times 10^{-11}\ m^{-1} s^{-1}$; $T_{m1} = 220\ K$, $T_{m2} = 260\ K$, $T_{mx} = 280\ K$.

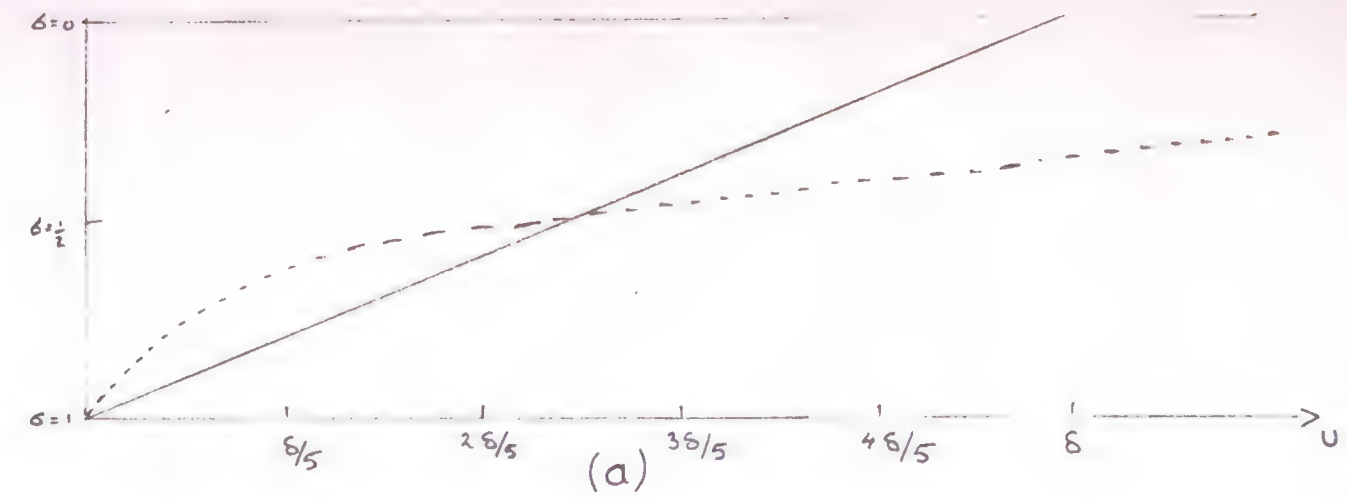


(a)

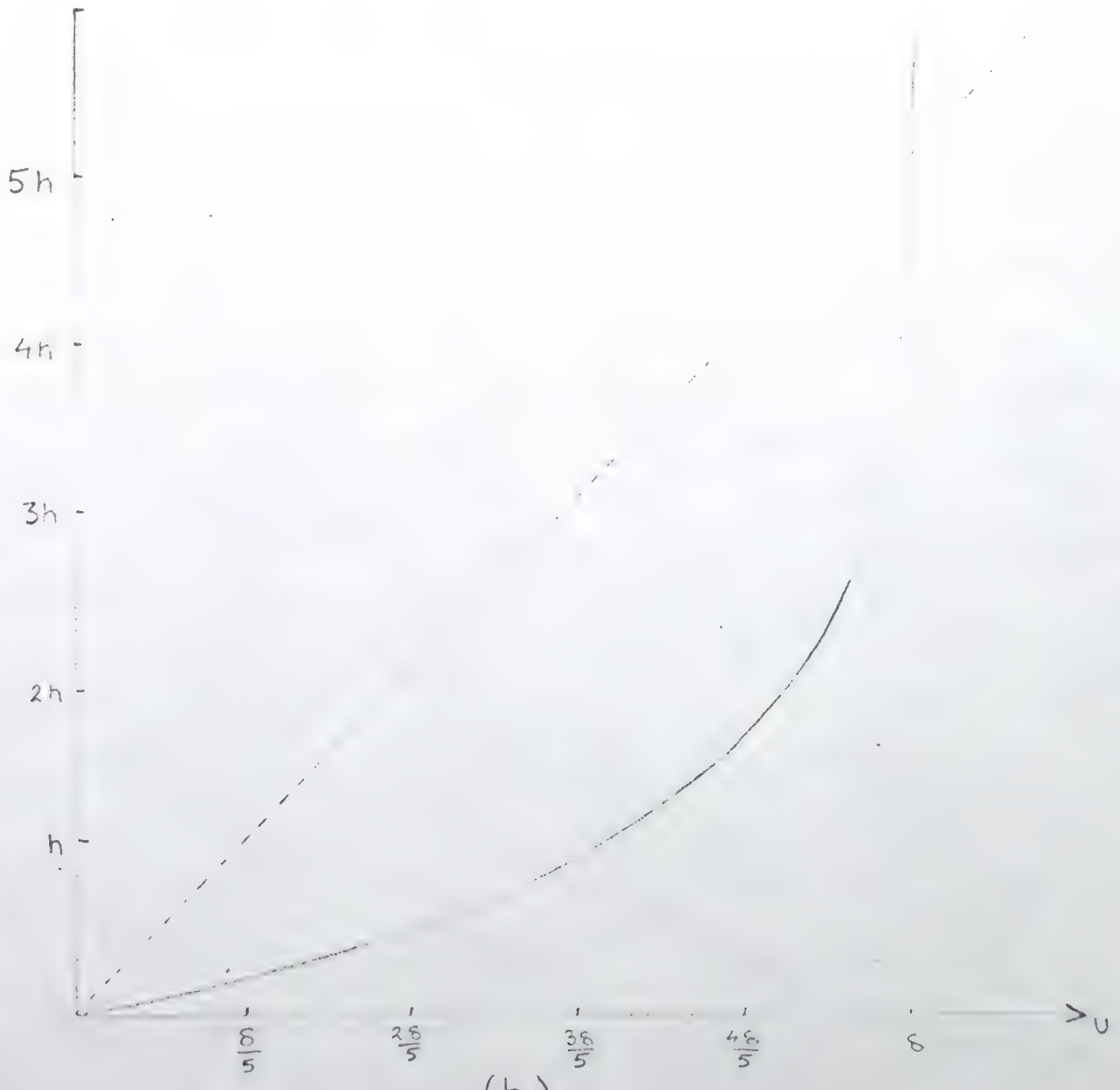


(b)

Figure 1

$\sigma = 0$ ---------- $(\psi = 0)$

level 1

$\sigma = 1/4$ ---------- $U, T_m, \frac{\partial T_m}{\partial y}$ ; $u, v, T$ $(\phi, \omega)$

$\sigma = 1/2$ ---------- $(\psi)$

level 2

$\sigma = 3/4$ ---------- $U, T_m, \frac{\partial T_m}{\partial y}$ ; $u, v, T$ $(\phi, \omega)$

$\sigma = 1$ ---------- $U_*, T_{m*}, \frac{\partial T_m}{\partial y}_*$ $(\psi = 0)$

Figure 2

Figure 3

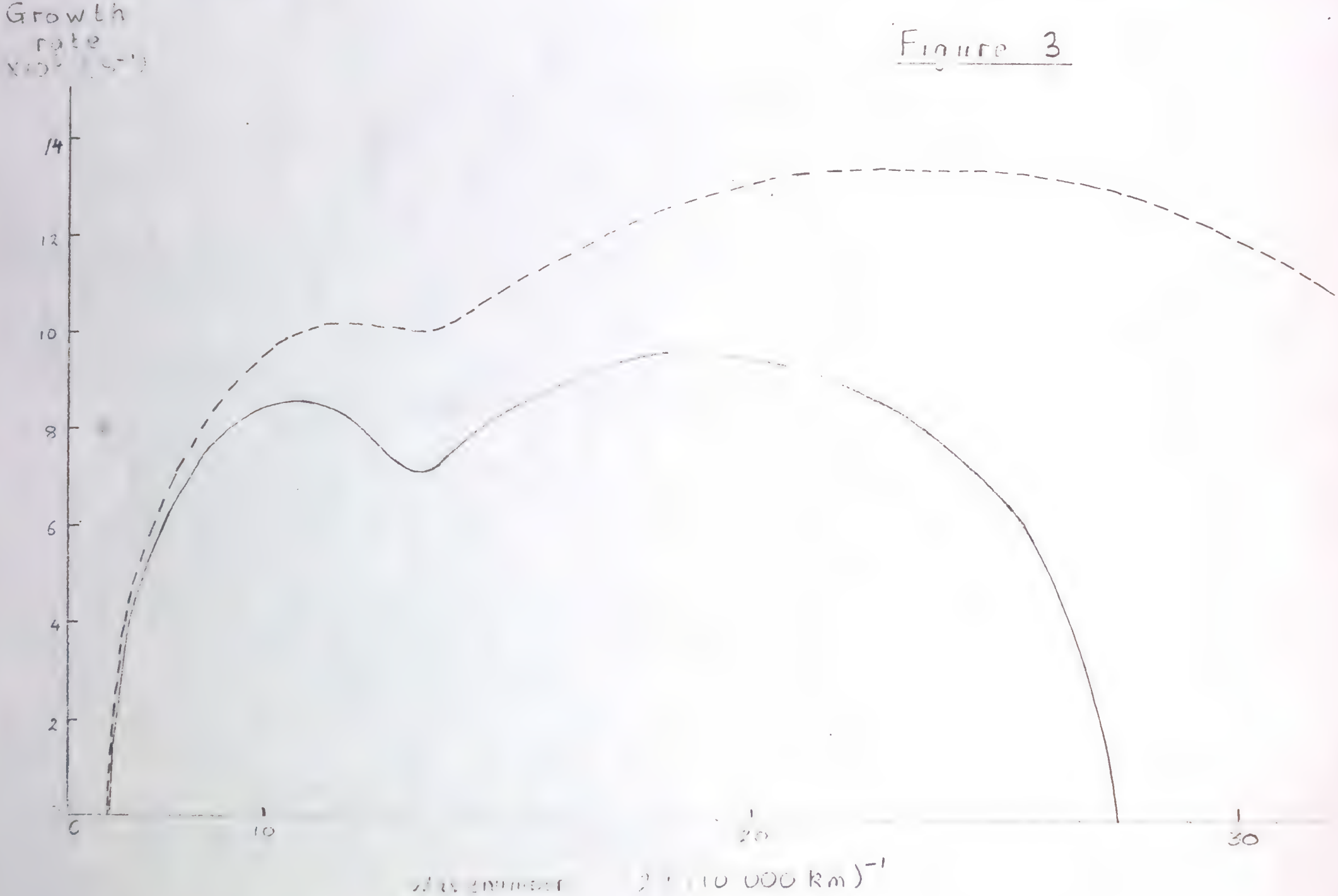

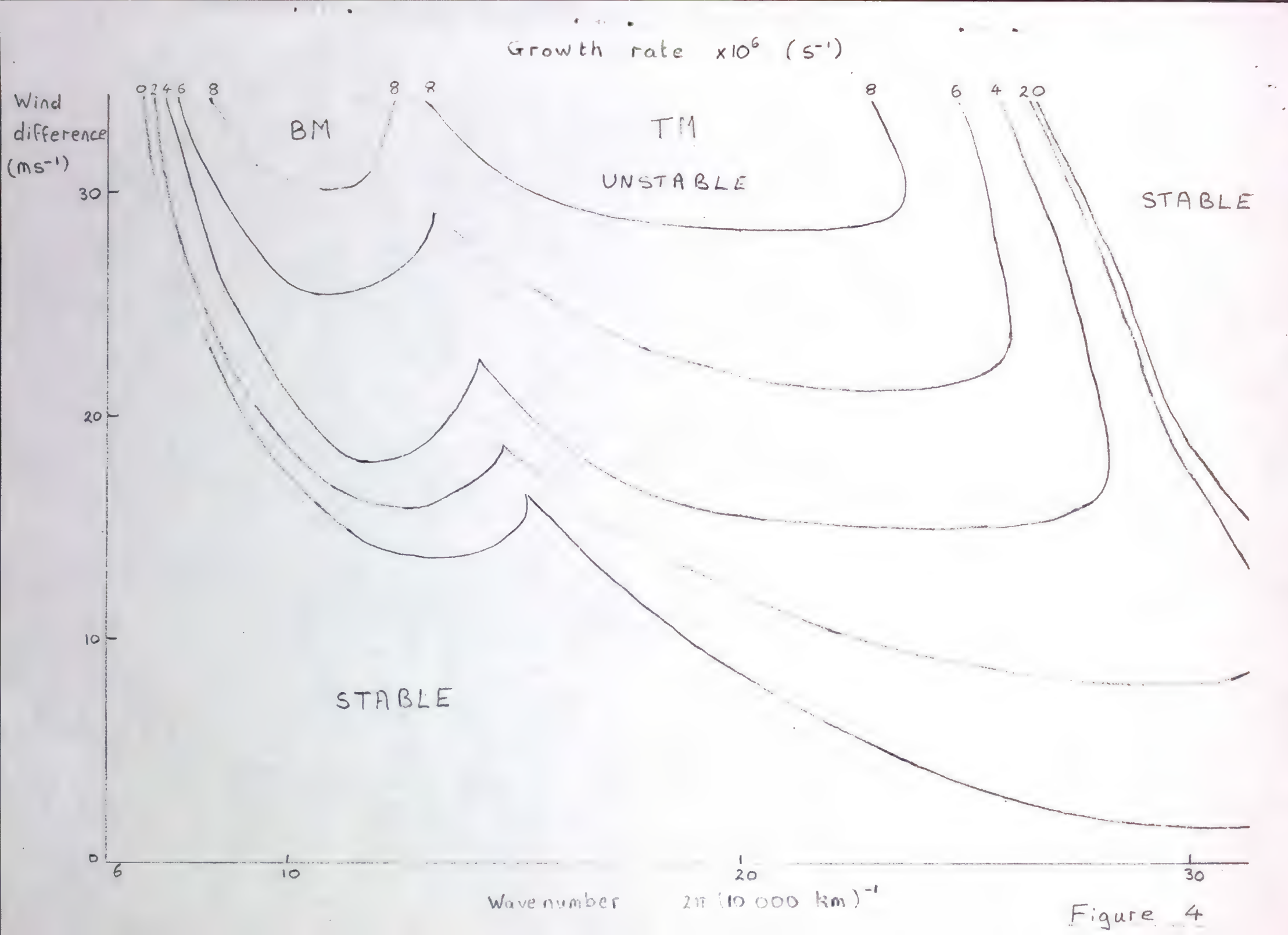
Growth rate x10⁶ (s⁻¹)
Wind difference (ms⁻¹)
0 2 4 6 8
8 8
8
6 4 20
BM
TM
UNSTABLE
STABLE
STABLE
30
20
10
0
6
10
1/20
1/30
Wavenumber 2π (10 000 km)⁻¹

Figure 4

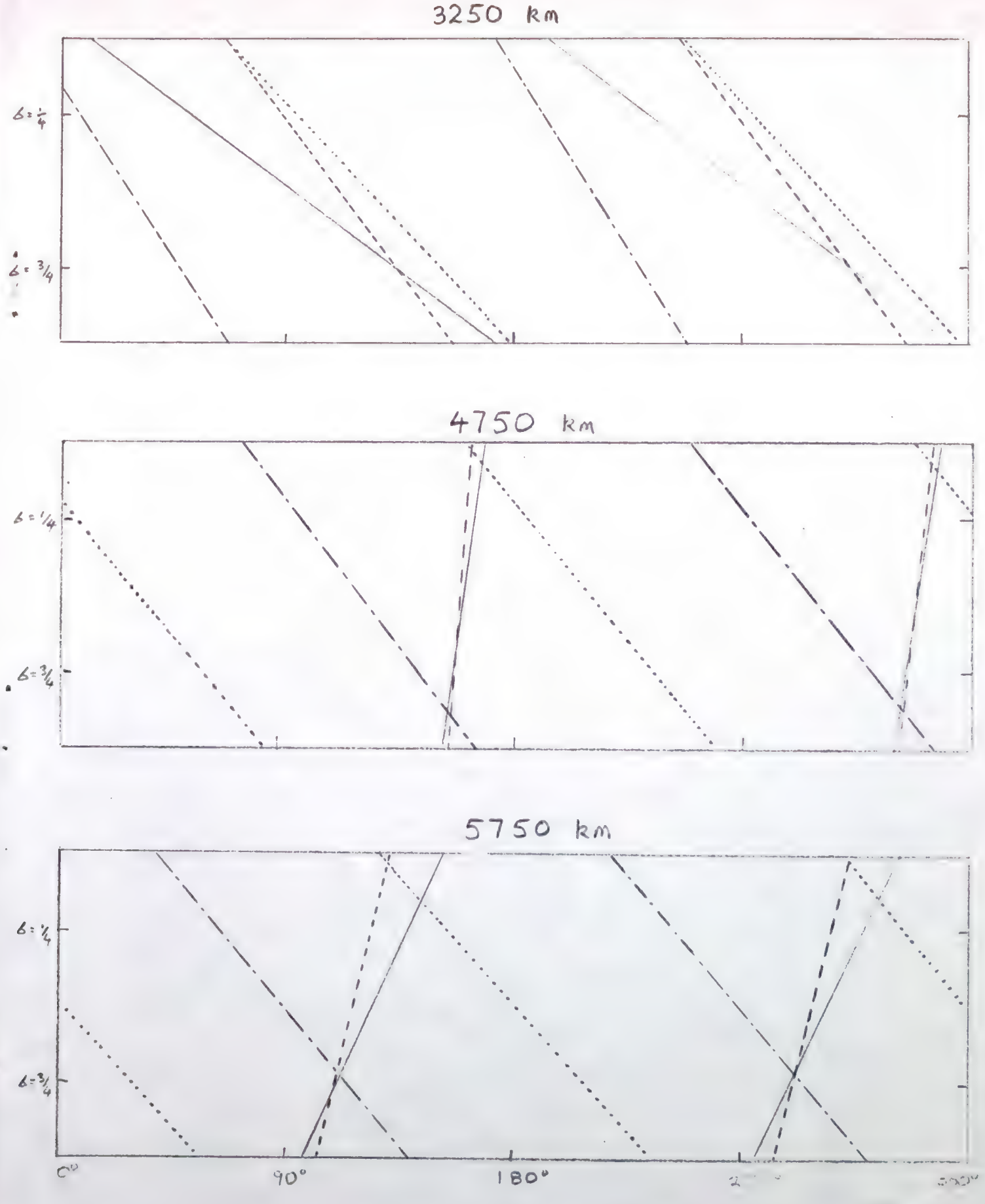
3250 km
δ = 1/4
δ = 3/4
4750 km
δ = 1/4
δ = 3/4
5750 km
δ = 1/4
δ = 3/4
0°
90°
180°
Phase angle

Figure 5

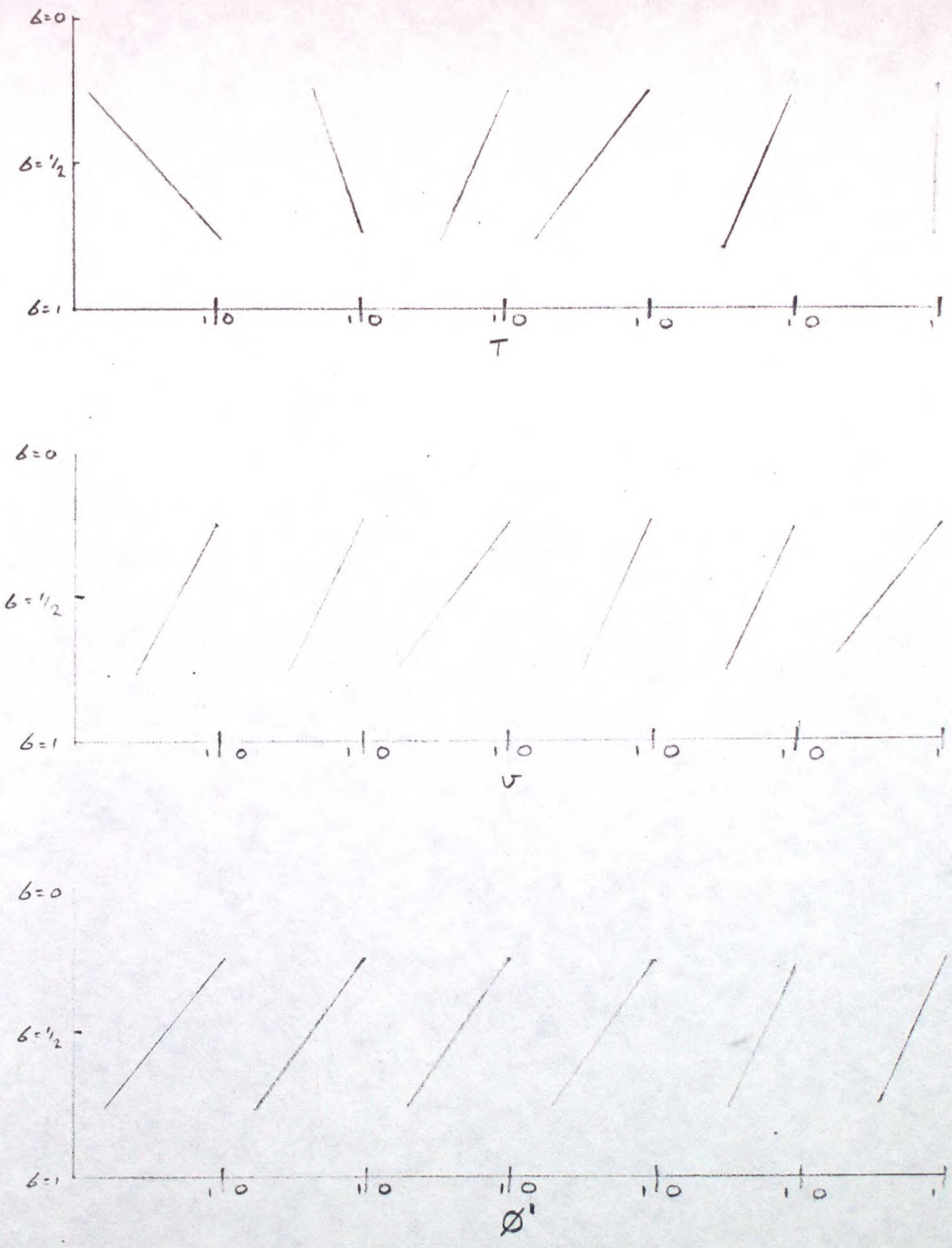
δ=0
δ=1/2
δ=1
T
δ=0
δ=1/2
δ=1
v
δ=0
δ=1/2
δ=1
Ø'
Stable
Start of TM
Max of TM
Minimum growth rate
Max of BM
Stop of BM

Figure 6

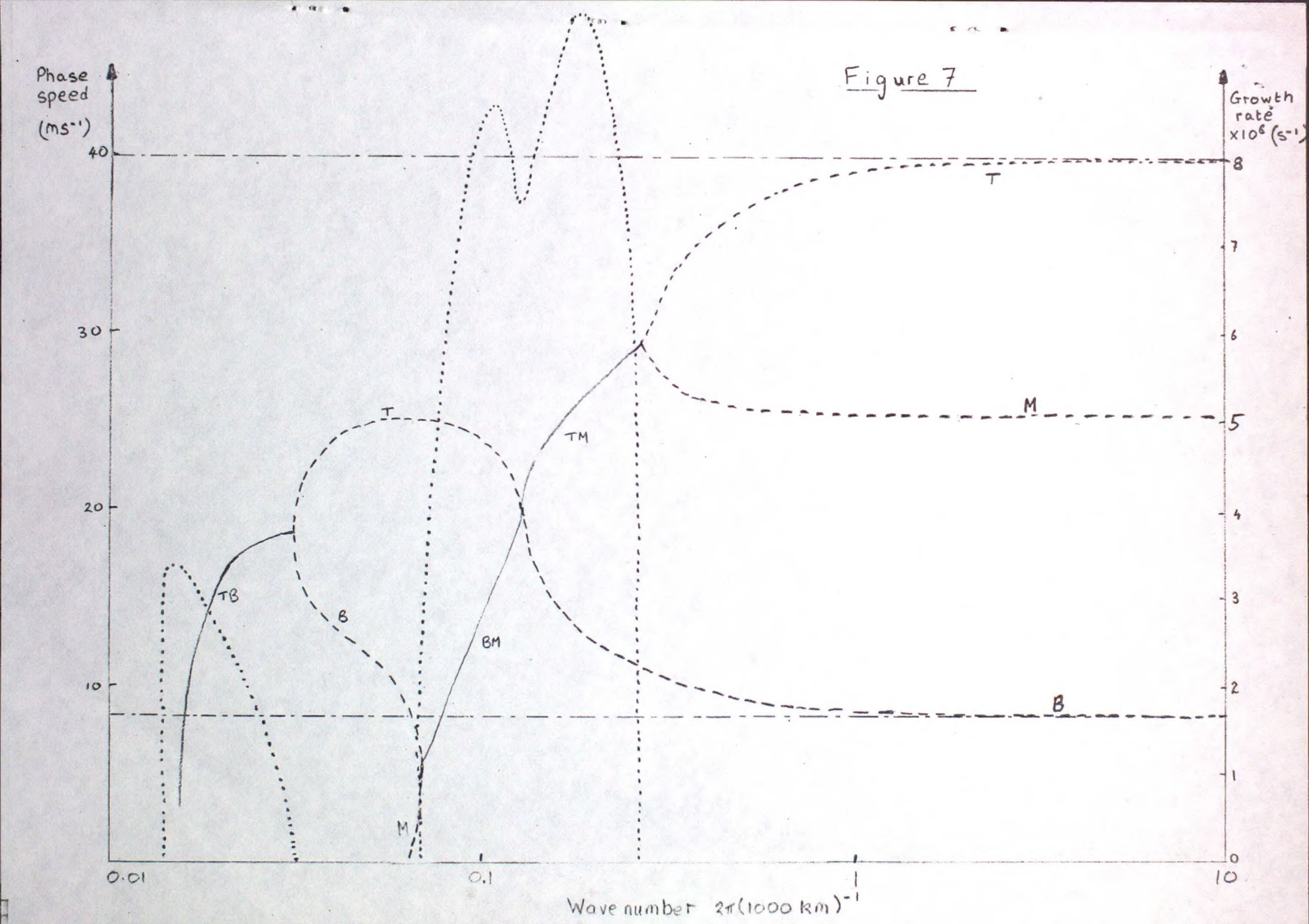
Figure 7
Phase speed (ms⁻¹)
Growth rate x10⁶ (s⁻¹)
40
30
20
10
8
7
6
5
4
3
2
1
0
T
M
B
TM
BM
TB
0.01
0.1
1
10
Wave number 2π(1000 km)⁻¹

Figure 8

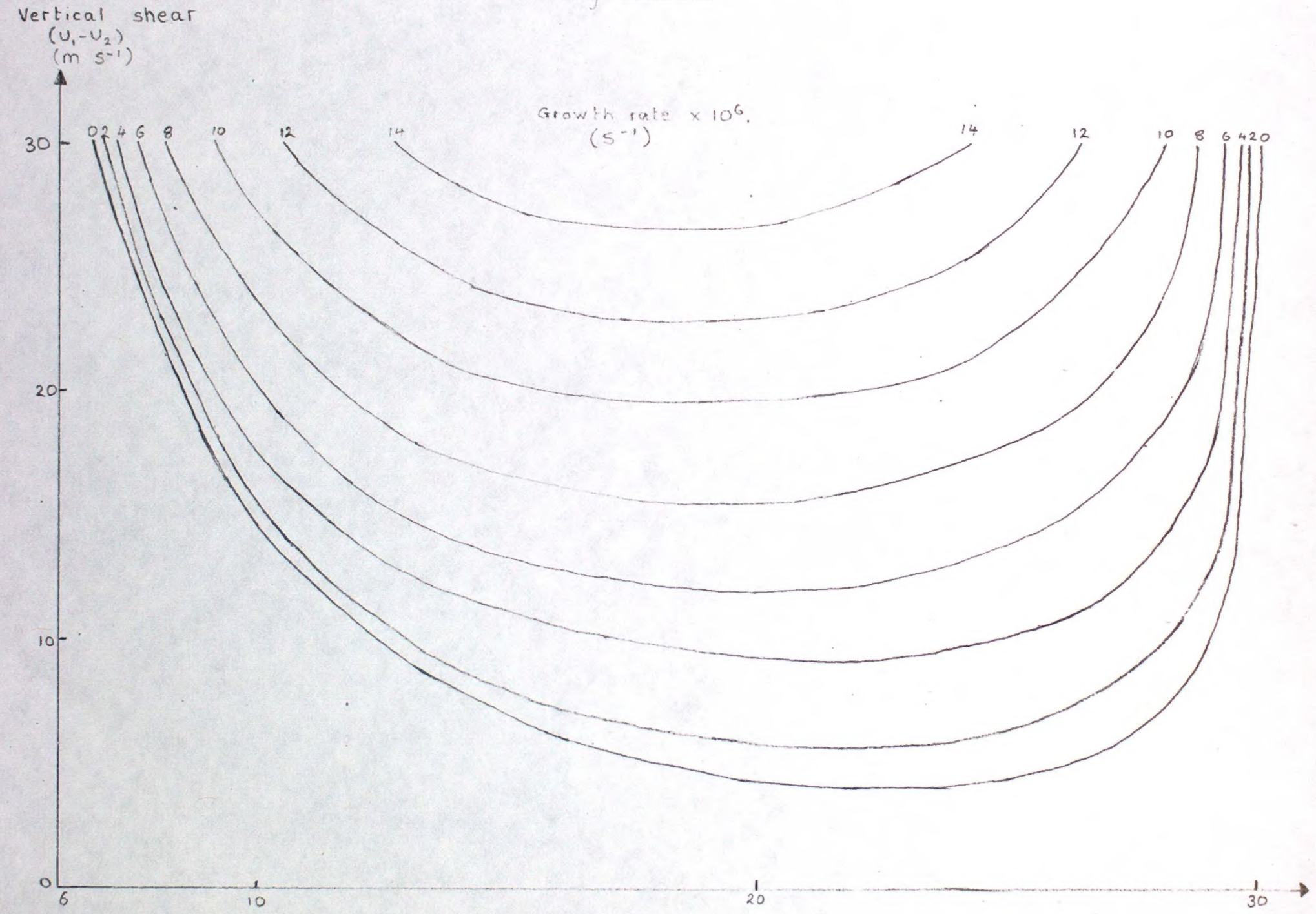
Vertical shear
$(U_1 - U_2)$
(m $s^{-1}$)
Growth rate $\times 10^6$.
($s^{-1}$)
0 2 4 6 8 10 12 14
14 12 10 8 6 4 2 0
30
20
10
0
6
10
20
30
Wave number (10000 km)$^{-1}$

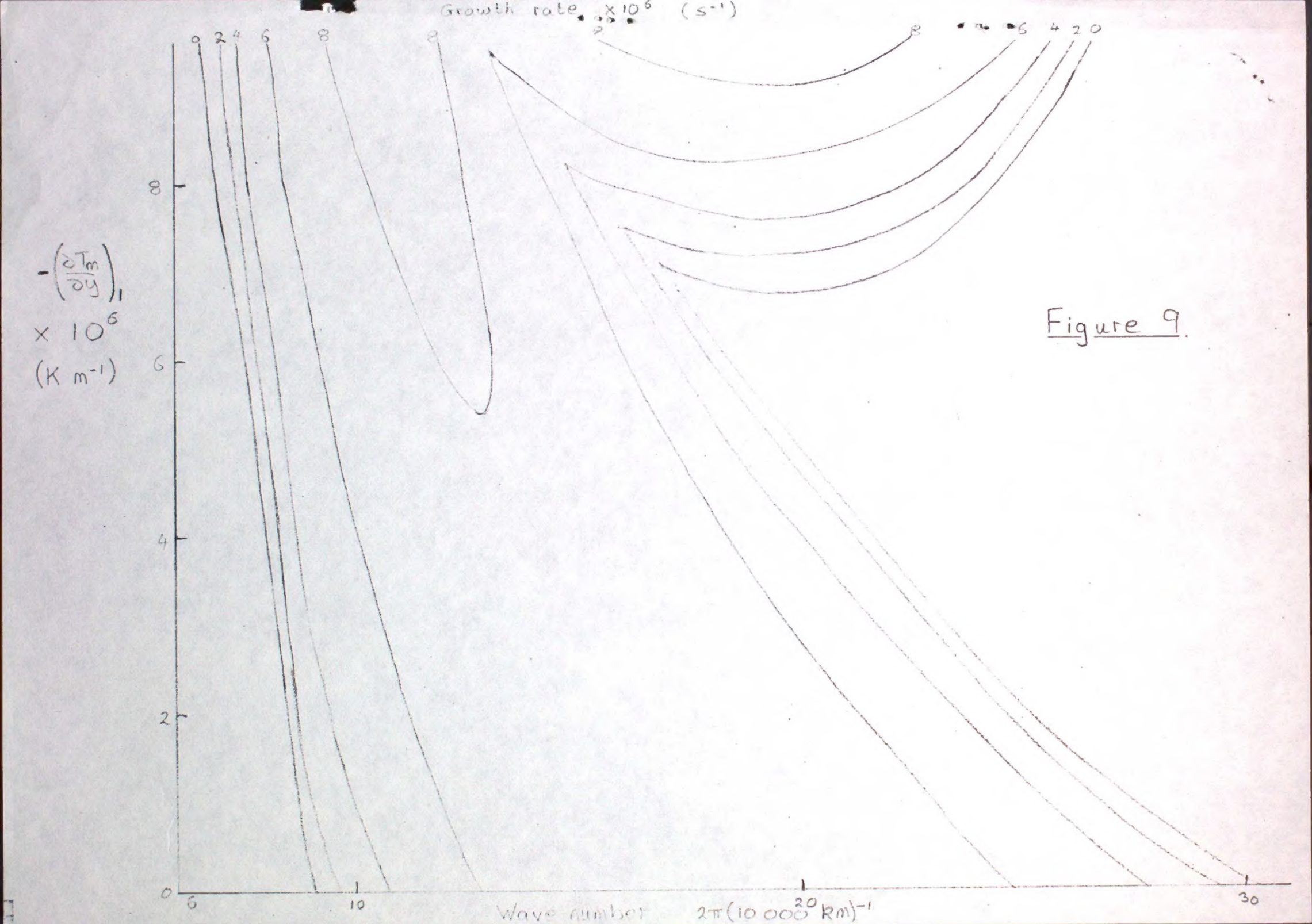

Growth rate $\times 10^6$ $(s^{-1})$
0 2 4 6 8 8 8 8 6 4 2 0
$-\left(\frac{\partial T_m}{\partial y}\right)_1$
$\times 10^6$
$(K\ m^{-1})$
0 2 4 6 8
6 10 20 30
Wave number $2\pi(10\,000\ km)^{-1}$


Figure 9.